Theor Chem Acc (2012) 131:1102
DOI 10.1007/s00214-012-1102-5

REGULAR ARTICLE

Molecular design and theoretical investigation on novel porphyrin derivatives for dye-sensitized solar cells

Hao Dong · Xin Zhou · Chunjie Jiang

Received: 1 June 2011 / Accepted: 25 July 2011 / Published online: 4 February 2012

Abstract We report on a quantum-chemical study of the electronic and optical properties of a series of β, β'-edge-fused zinc porphyrin with different aromatic rings, in order to design efficient sensitizers for dye-sensitized solar cells (DSSCs). Our calculations found that the replacement of quinoxaline moiety in **ZnQMA** (having high power conversion efficiency η of 6.3%) with other aromatic rings decreases the HOMO–LUMO energy gap mainly due to destabilization of the HOMO level. For all of the investigated compounds, the reorganization energies of electron and hole are in the same order of magnitude as and similar to those of **ZnQMA**. The absorption spectra in both Soret and Q bands for most of the considered molecules exhibit red shifts to some extent with respect to that of **ZnQMA**. In the simulated dye-sensitized TiO_2 systems, the bidentate adsorption mode of porphyrin derivatives is computed to be energetically favored compared to the monodentate one, which well confirms the experimental results observed by X-ray photoelectron spectroscopy. The slightly shorter Ti–O bond lengths calculated for **D**–TiO_2 systems point toward a stronger interaction of the dye with the titania surface compared to **ZnQMA**–TiO_2 systems. Our calculation indicates that the designed molecule **D** is promising to challenge the current photoelectric conversion efficiency record 6.3% of **ZnQMA**.

H. Dong · C. Jiang (✉)
Institute of Chemistry for Functionalized Material, College of Chemistry and Chemical Engineering, Liaoning Normal University, Dalian 116029, China
e-mail: jiangcj@lnnu.edu.cn

X. Zhou (✉)
State Key Laboratory of Catalysis, Dalian Institute of Chemical Physics, Chinese Academy of Sciences, Dalian 116023, China
e-mail: xzhou@dicp.ac.cn

Keywords Dye-sensitized solar cells · Molecular design · Porphyrin · Density functional calculations

1 Introduction

In today's global challenge to capture and utilize solar energy for a large-scale sustainable development, dye-sensitized solar cells (DSSCs) represent a highly promising approach to the direct conversion of light into electrical energy at low cost and with high efficiency [1–4]. At present, DSSCs based on ruthenium(II)-polypyridyl complexes as the active material have an overall power conversion efficiency (η) exceeding 11% under standard (Global Air Mass 1.5) illumination [5–8]. However, their extensive application would be hampered considerably owing to the limited availability and high cost of ruthenium metal. Many efforts have been devoted to develop new and efficient sensitizers suitable for practical use. Among them, organic sensitizers without metal or with inexpensive metal have been investigated extensively because of their modest cost, ease of synthesis and modification, large molar absorption coefficients, and satisfactory stability [9, 10]. So far, many organic dyes exhibiting relatively high DSSCs performance have been designed and developed, such as coumarin [11–14], polyene [15–17], hemicyanine [18, 19], thiophene-based [20–22], indoline [23, 24], perylene [25, 26], squaraine [27–29], phthalocyanine [30–32], etc.

Among organic-based dyes, porphyrins have attracted much attention owing to their intrinsic advantages such as their rigid molecular structure with large absorption coefficients in the visible region and their many reaction sites, i.e., four *meso* and eight β positions, available for functionalization. Nevertheless, the insufficient light-harvesting properties relative to the ruthenium complexes have limited

the cell performance of porphyrin-sensitized solar cells. Broadening and red-shift of absorption bands together with an increasing intensity of the Q bands compared to that of the Soret band are promising strategies to solve the above problem. For example, elongation of the π conjugation and loss of symmetry in porphyrin carboxylic acid increased the power conversion efficiency by 50% relative to the nonfused counterpart [33]. Campbell and crew successfully designed the extended porphyrin π-system by substituting the β-pyrrolic position with an olefin-linked electron acceptor, which shows a high photoelectronic conversion efficiency of 7.1% [34]. Kim and co-workers estimated the relative positions of the HOMO and LUMO levels in the donor and acceptor moieties of porphyrin derivatives by using AM1 and DFT calculations. Their result suggests that the charge-separated state is one of the main factors influencing solar cell efficiency [35, 36]. Zhang et al. theoretically designed and investigated many kinds of substituted porphyrins with different donor–acceptor combinations. They pointed out a higher efficiency than 7.1% may be obtained with these novel porphyrin derivatives [37, 38]. Recently, Bessho et al. [39] reported the achievement of 11% efficiency based on a D-π-A type dye in which the porphyrin itself constitutes the π bridge. This breakthrough indicated that the porphyrins are highly promising dyes in DSSCs.

Constructing β, β'-edge-fused zinc porphyrin with quinoxaline moiety has been found to be another promising way to improve the cell performance [40, 41]. High η value (6.3%) of mono-carboxyquinoxalino[2,3-β]porphyrins (**ZnQMA**) has been obtained, further confirming the influence of the light-harvesting properties in the improvement in the cell performance of porphyrin-sensitized solar cells. Further optimization of this kind of porphyrin derivative may be a fruitful source of getting improved conversion efficiency. We wondered whether replacement of the quinoxaline moiety in **ZnQMA** with other aromatic rings would tune the positions of HOMO and LUMO, increase the relative intensities of Soret and Q bands, and be promising to challenge the current photoelectric conversion efficiency 6.3% of **ZnQMA**. Our computational investigation of this question was motivated by the recent report by Muranaka and co-workers of azulene-fused tetraazaporphyrin, named azulenocyanine with intense near-IR absorption [42]. They found that the azulene unit significantly lowers the LUMO level of the macrocycle due to the electron-accepting nature of the seven-membered azulene skeleton and modestly destabilizes the HOMO level, which makes a small HOMO–LUMO gap.

In this work, we report on density functional theory calculations on the porphyrin derivatives isolated and adsorbed on TiO_2 clusters. Firstly, a detailed description of the computational tools employed is introduced. Secondly, a discussion of the obtained geometrical and electronic properties of isolated porphyrin molecules based on the comparison with the available experimental data is presented. Thirdly, the interaction between the porphyrin dyes and TiO_2 clusters is investigated. Finally, the main conclusions are exposed.

2 Computational methodology

The ground-state and lowest singlet exited-state geometries of the isolated molecules have been fully optimized with the three-parameter functional of Becke and the correlation functional of Lee, Yang, and Parr (B3LYP) [43, 44]. B3LYP vibrational analyses were performed at each stationary point, in order to confirm its identity as a minimum. Full geometry optimization for each molecule in their anionic and cationic states was also completed with the density functional theory. All open-shell calculations were performed using unrestricted methods, and spin contamination in the radical species was found to be very small ($\langle S^2 \rangle \leq 0.79$). The impact of the different computational levels on the molecular properties was also checked by carrying out additional geometry optimizations on zinc meso-tetraphenylporphyrin (**ZnTPP**) and excitation energy calculations on **ZnQMA**, using the MPW1 K [45] and PBE0 [46] x-c DFT functionals. All calculations were performed using the Gaussian 09 suite of programs [47] with the standard 6-31G(d) basis set [48], which has already been proved to be an optimal compromise between accuracy and computational cost for large aromatic molecules [49].

TDDFT [50] calculations with B3LYP/6-31G(d) level have been performed to calculate the excitation energies at the optimized geometries of the ground states and the lowest singlet excited states of the isolated molecules in order to simulate the absorption and fluorescence spectra. In this case, the 50 lowest singlet–singlet excitation energies were computed. The absorption spectra were simulated by fitting to a Gaussian line shape with a half-width at half-maximum of 20 nm. Solvent effects were considered in the framework of the self-consistent reaction field polarizable continuum model (PCM) [51].

The majority of the experimental investigations on the interfacial electron-transfer in the dye-sensitized TiO_2 systems are carried out with TiO_2 nanoparticles that are a mixture of the rutile and anatase crystal forms of TiO_2 with a variety of exposed surfaces. Theoretically, in order to study electronic structure of the dye-sensitized TiO_2 systems and to understand character of the states involved in the dye molecule to semiconductor charge-transfer process, several research groups used different models to simulate

the TiO_2 nanoparticles. De Angelis et al. [52–54] used a Car-Parrinello approach to optimize the structures of the stoichiometric anatase TiO_2 (101) surface with $(TiO_2)_{38}$ and $(TiO_2)_{82}$ clusters. Guo et al. [55] studied the ultrafast electron-transfer processes in three dye-sensitized TiO_2 systems (pycooh-, catechol-, and alizarin-) by using different sizes of TiO_2 clusters from $(TiO_2)_8$ to $(TiO_2)_{16}$. Recently, Sanz et al. examined the structural and electronic properties of the alizarin dye supported on TiO_2 nanoclusters by means of time-dependent density functional calculations performed in the time-domain framework. They found that a unit of $(TiO_2)_6$ as the minimal nanocluster model is able to simulate semi-quantitatively all the features in the electronic structure of the system [56].

Based on the reported results in the above literatures, we have chosen $(TiO_2)_8$ cluster as a good tradeoff between accuracy and computational convenience, whose structure is taken from literature [55] to substitute TiO_2 nanocrystals in order to examine the effect of semiconductor. We regard this cluster as a reasonable choice for its actual geometry, so we have not paid any effort to find the absolute energy minimum for the $(TiO_2)_8$ cluster. We have performed full optimization on TiO_2–dye complexes without symmetry constraints at the B3LYP/6-31G(d) theory level.

3 Results and discussion

In order to choose a relatively reliable method to calculate the geometries and electronic structures of molecules which we are interested in, we have investigated the effects of functional on the geometry parameters of ZnTPP and the excitation energies of **ZnQMA**. In this paper, B3LYP, MPW1 K, and PBE0 are used to make the comparison because they are proven to be good to descript the electronic properties of organic dyes used in DSSCs [56–58]. The computed and experimental key geometric parameters of **ZnTPP** are collected in Table 1. By comparing the main geometry parameters calculated by different functionals with available X-ray structure data, it turns out B3LYP can be a good choice of functional for geometry optimization. In addition, the calculated and experimental absorption maxima in Q and Soret bands of **ZnQMA** shown in Table 2 indicate that all of functionals do not reproduce the experimental absorption around 620 nm. From Table 2, a red shift of the calculated absorption spectra (7–17 nm) is observed on going from the gas phase to CH_2Cl_2 solution. The simulated absorption spectra by B3LYP including solvent effect exhibits better agreement than other functionals with the experimental values. Therefore, we employ the B3LYP/6-31G(d) for the subsequent investigations.

3.1 Optimized geometrical structures at the ground (S0) and first excited states (S1) of the isolated porphyrin compounds

Previous theoretical investigations on dye sensitizers have shown that inclusion of the solvation effects is crucial when describing the electronic structure and absorption spectra of dye molecules [62, 63]. So in this work, the main geometric parameters at the ground state and the lowest single excited state optimized with the level of B3LYP/6-31G(d) in CH_2Cl_2 solution are listed in Table 3. And the sketch map of the investigated molecular structures is depicted in Fig. 1. The excited-state structural parameters of **E** were excluded because the optimization of its excited-state has not been converged. The calculated data in Table 3 indicate the main geometric parameters of zinc porphyrin in both the ground state and the excited state are marginally affected by the different fused aromatic rings: the difference in bond lengths is smaller than 0.03 Å, and the change in bond angles is less than 3°. At the ground state, the porphyrin and fused aromatic rings are fully conjugated as demonstrated by the negligible dihedral angles between them in **ZnQMA**, **A**, **B**, and **C**. The most significant differences in geometry are found for the dihedral angle between the porphyrin ring and the aromatic moiety for **D** and **E**, in which not only the porphyrin ring and the fused ring are not coplanar, but also the aromatic moieties are distorted. So the average dihedral angles between these two rings are listed in Table 3. The dihedral angles between two parts are about 22° in the case of **D** and 70° for **E** at the ground state, and distorted angles become bigger in the excited state.

3.2 Electronic structures of isolated porphyrin molecules

3.2.1 Frontier molecular orbitals

A schematic representation of the energy levels for all the investigated molecules calculated in CH_2Cl_2 solution is reported in Fig. 2. Corresponding data of HOMOs, LUMOs, and HOMO–LUMO gaps are listed in Table 4. Early theoretical interpretations of the spectra of various metalloporphyrins have been made by Gouterman et al. [64] who initially used the four-orbital model to interpret the Q and B bands, which assumes that the HOMO and HOMO−1 are almost degenerate in energy and well separated from the other levels, and a similar assumption is made for the LUMO and LUMO+1. As shown in Fig. 2, visible separations between the two highest occupied orbitals and two lowest unoccupied orbitals result in the fact that the four-orbital model no longer holds for these molecules.

Table 1 Geometric parameters (in Å and °) of zinc meso-tetraphenylporphyrin (**ZnTPP**) calculated in vacuo using a 6-31G(d) basis set at different methods

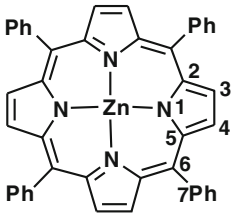

Geometric parameters	B3LYP	MPW1 K	PBE0	Exp.
r(Zn-N1)	2.040	2.022	2.029	2.036[a]
r(N1-C2)	1.377	1.360	1.369	1.375[a]
r(C2-C3)	1.445	1.435	1.440	1.443[a]
r(C3-C4)	1.361	1.351	1.358	1.351[a]
r(C5-C6)	1.405	1.393	1.400	1.399[a]
r(C6-C7)	1.502	1.490	1.494	1.500[a]
α(C2-N1-C5)	106.5	106.5	106.3	106.8[b]
α(Zn-N1-C2)	126.8	126.7	126.9	126.3[c]
α(C4-C5-C6)	124.4	124.2	124.2	125.0[c]
α(N1-C5-C6)	125.8	125.9	125.7	126.3[c]
α(C5-C6-C7)	117.6	117.6	117.6	117.2[b]

[a] Ref. [59], [b]Ref. [60], [c]Ref. [61]

Table 2 Calculated and experimental UV–visible absorption spectra in both vacuum and solvent (CH_2Cl_2) of **ZnQMA**

Molecule	B3LYP/6-31G(d)		MPW1 K/6-31G(d)		PBE0/6-31G(d)		Exp.
	Vacuum λ^{max} (*f*)	Solvent λ^{max} (*f*)	Vacuum λ^{max} (*f*)	Solvent λ^{max} (*f*)	Vacuum λ^{max} (*f*)	Solvent λ^{max} (*f*)	λ^{max} (ε)
ZnQMA	387.8 (1.681)	405.6 (1.884)	392.8 (0.868)	409.0 (1.131)	376.5 (1.609)	393.6 (2.036)	415 (183.7)
	571.1 (0.025)	584.3 (0.054)	536.9 (0.028)	541.3 (0.039)	558.6 (0.023)	562.2 (0.050)	578 (13.6)
							622 (12.6)

The calculated energy gap between the HOMO and LUMO is 2.58 eV for **ZnQMA**. Except **C**, the energy gaps of the molecules are smaller than that of **ZnQMA**. The order of the energy gaps is **E** (2.17 eV) < **B** (2.23 eV) < **D** (2.34 eV) < **A** (2.38 eV) < **C** (2.66 eV). Previous studies indicate that to some extent, the smaller the HOMO–LUMO gap of the sensitizer, the higher the efficiency of corresponding solar cell [37]. According to these studies, our designed molecules **A**, **B**, **D**, and **E** maybe exhibit higher efficiency than **ZnQMA** in DSSCs. From Fig. 2 and Table 4, the decrease in HOMO–LUMO energy gap mainly comes from the raise of HOMO by 0.26–0.5 eV. The replacement of the quinoxaline moiety with different aromatic rings negligibly affects the level of LUMO (less than 0.04 eV) except compound **C**.

In DSSCs, LUMO of the dye molecule should be higher in energy than the semiconductor conduction band edge and close to it. The electronic coupling strength between dye's LUMO and the semiconductor conduction band is a key property for an efficient electron injection from the dye onto the semiconductor surface. Since experiments show that **ZnQMA** has a high photoelectronic conversion efficiency of 6.3% [40, 41], the LUMO of **ZnQMA** is supposed to lie well above the TiO_2 conduction band edge, and the electronic coupling between them should be strong. On the basis of the present calculations, the LUMO energy of molecules **A**, **B**, **D** and **E** is almost the same as that of **ZnQMA**, so the alignment of the LUMO energy in these compounds with the TiO_2 conduction band edge is expected to be very similar with that in **ZnQMA**. In this aspect, our designed molecules **A**, **B**, **D** and **E** should be the suitable sensitizers for TiO_2.

Figure 2 illustrates the electron density distributions of all the considered molecules in their respective HOMO and LUMO. For all of the considered complexes, the pattern of the frontier orbitals is qualitatively similar. The electron density distribution of LUMOs around an anchoring group is known to influence the electronic coupling between the excited adsorbed dye and 3d orbital of TiO_2 [65]. By looking at Fig. 2, one can find that the carboxylic acids and

Table 3 Selected optimized geometrical parameters (in Å and °) computed for all molecules at the ground (S_0) and first excited states (S_1) in CH_2Cl_2 solution

Geometric parameters	**ZnQMA**		**A**		**B**		**C**		**D**		**E**
	S_0	S_1	S_0	S_1	S_0	S_1	S_0	S_1	S_0	S_1	S_0
r(Zn-N1)	2.118	2.062	2.074	2.043	2.104	2.077	2.123	2.117	2.126	2.125	2.116
r(Zn-N2)	2.024	2.025	2.035	2.044	2.010	2.016	2.009	2.011	1.996	2.002	2.012
r(Zn-N3)	2.063	2.069	2.054	2.052	2.075	2.075	2.069	2.073	2.075	2.075	2.064
r(Zn-N4)	2.025	2.023	2.036	2.044	2.018	2.019	2.009	2.012	1.998	2.001	2.007
r(N1-C5)	1.378	1.408	1.392	1.401	1.382	1.371	1.379	1.386	1.381	1.389	1.375
r(N1-C6)	1.380	1.366	1.390	1.400	1.389	1.414	1.378	1.386	1.375	1.375	1.373
r(N2-C7)	1.374	1.388	1.376	1.382	1.374	1.383	1.373	1.380	1.375	1.375	1.368
r(N2-C8)	1.385	1.367	1.381	1.373	1.385	1.374	1.387	1.384	1.385	1.387	1.388
r(N3-C9)	1.375	1.388	1.376	1.378	1.373	1.381	1.374	1.377	1.372	1.378	1.373
r(N3-C10)	1.375	1.363	1.377	1.377	1.376	1.369	1.375	1.378	1.374	1.371	1.374
r(N4-C11)	1.385	1.391	1.381	1.373	1.384	1.384	1.387	1.383	1.384	1.383	1.388
r(N4-C12)	1.375	1.364	1.376	1.382	1.374	1.372	1.373	1.382	1.375	1.380	1.369
r(C5-C13)	1.463	1.458	1.439	1.419	1.443	1.449	1.471	1.462	1.472	1.439	1.490
r(C6-C14)	1.464	1.472	1.440	1.425	1.468	1.437	1.472	1.465	1.474	1.477	1.491
r(C13-C14)	1.431	1.405	1.394	1.393	1.415	1.426	1.430	1.434	1.421	1.445	1.462
α(N1-Zn-N2)	90.0	90.6	90.3	90.5	89.7	90.0	90.3	90.3	90.4	90.2	89.5
α(N2-Zn-N3)	90.0	89.3	89.7	89.5	89.6	89.5	89.8	89.7	89.6	89.8	89.9
α(N3-Zn-N4)	90.0	89.3	89.7	89.4	89.2	88.8	89.8	89.7	89.7	89.5	90.0
α(N4-Zn-N5)	90.0	90.8	90.3	90.6	91.4	91.8	90.2	90.3	90.4	90.5	89.8
α(Zn-N1-C5)	125.0	125.9	125.1	125.8	123.4	123.7	125.4	125.7	125.3	125.4	126.0
α(Zn-N1-C6)	125.0	126.6	125.3	125.9	127.7	128.2	125.3	125.6	126.0	125.8	124.9
α(Zn-N2-C7)	127.1	125.9	126.9	126.6	126.3	126.0	126.6	126.6	126.2	126.5	126.2
α(Zn-N2-C8)	126.6	127.7	126.8	127.1	127.1	127.3	126.9	127.1	127.1	126.9	126.8
α(Zn-N3-C9)	126.8	126.6	126.8	126.8	126.8	126.6	126.9	126.9	126.9	126.8	127.0
α(Zn-N3-C10)	126.8	127.1	126.8	126.8	127.0	127.2	126.9	126.9	126.9	127.0	126.3
α(Zn-N4-C11)	126.5	127.3	126.8	127.1	127.3	127.7	126.9	127.1	127.0	126.9	126.0
α(Zn-N4-C12)	127.1	126.2	126.9	126.5	126.3	125.8	126.7	126.6	126.3	126.2	126.7
α(C5-N1-C6)	110.0	107.5	109.6	108.4	108.9	108.1	109.3	108.7	108.6	108.7	109.0
d(por-aroma)[a]	0.3	0.6	0.0	0.1	0.3	7.9	0.0	1.1	22.2	39.7	70.2

For labeling, refer to Fig. 1

[a] *d*(por-aroma) is the average dihedral angle between the zinc-porphyrin ring and the fused aromatic moiety

the connecting carbon atoms of molecules **A**, **B**, **D**, and **E** possess comparable and even larger electron densities with respect to those in the LUMO of **ZnQMA**, which may lead to competitive and even higher cell performance of these four designed molecules relative to that of **ZnQMA** [41].

3.2.2 Reorganization energy

One of the biggest challenges for developing organic-dye-based DSSCs is relatively low efficiency, which depends sensitively on the peculiar charge-transfer character of the lowest excited state in the dye. In general, organic π-conjugated materials are assumed to transport charge at room temperature via a thermally activated hopping-type mechanism [66, 67]. In this model, the charge transport is the intermolecular process in which the charge hops between two molecules, which can be summarized as follows:

$$M^{+/-} + M \rightarrow M + M^{+/-}$$

where M is the neutral molecule interacting with neighboring oxidized or reduced $M^{+/-}$. At the microscopic level, the charge transport mechanism can be described as a self-exchange transfer process, in which an electron or hole transfer occurs from one charged molecule to an adjacent neutral molecule. The rate of intermolecular charge transfer (K_{et}) can be estimated from semi-classical Marcus theory [68, 69] given in

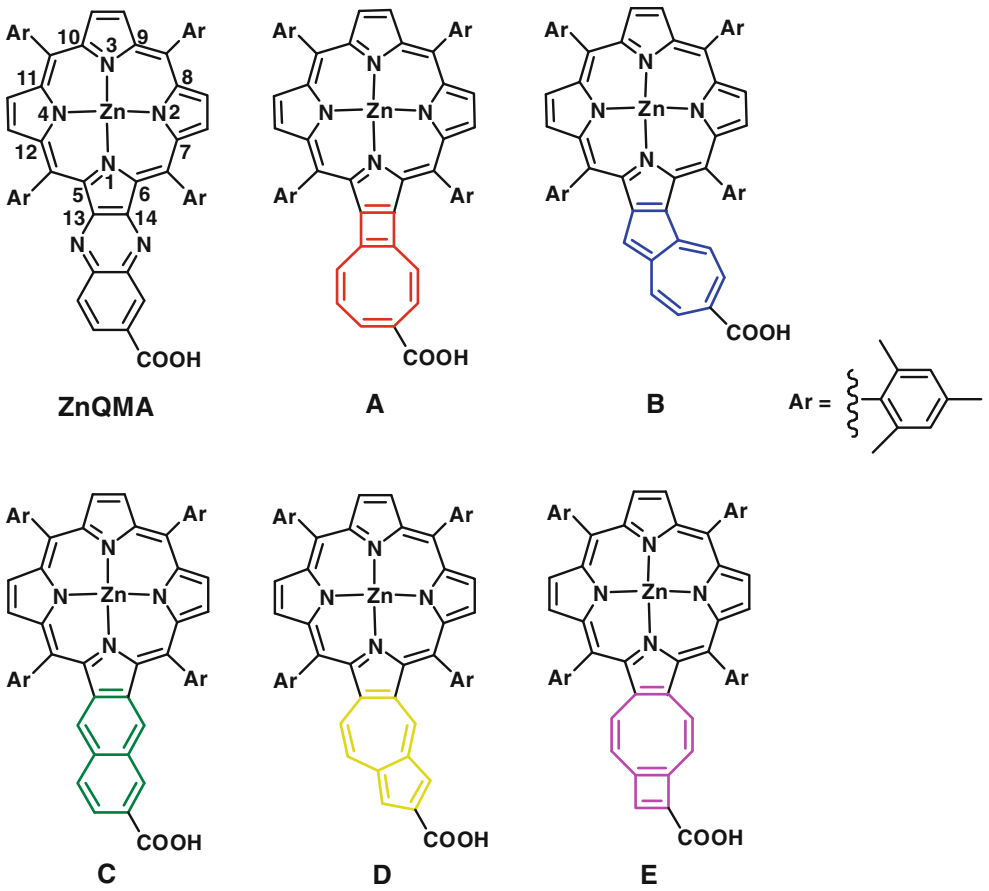

Fig. 1 Molecular structures of the investigated molecules

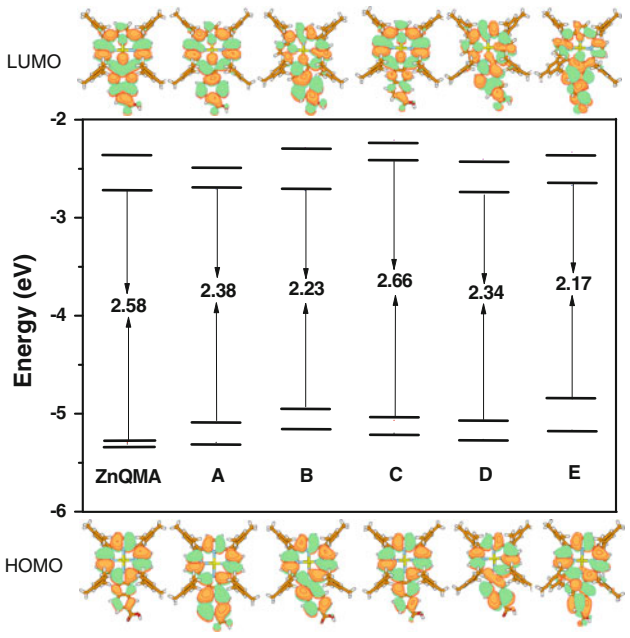

Fig. 2 Molecular orbital energy levels (eV) of all the investigated molecules obtained in CH_2Cl_2 solution

$$K_{et} = A \exp\left[\frac{-\lambda}{4K_B T}\right]$$

where T is the temperature, A is a prefactor related to the electronic coupling between adjacent molecules, λ is the reorganization energy and K_B is the Boltzmann constant. It will be seen that variations in the reorganization energies, which have an exponential barrier, dominate the changes in overall carrier transfer rates as the molecular structures are varied. For efficient charge transport, the reorganization energy needs to be small. At this stage, we focus our discussion on the reorganization energy.

In general, the λ value is determined by fast changes in molecular geometry (the inner reorganization energy) and by slow variations in solvent polarization of the surrounding medium (the external contribution). In the case of the active organic π-conjugated systems, the latter contribution can be neglected, so that the former becomes the dominant. Hence, the reorganization energy for hole/electron can be defined as follows:

$$\lambda_{hole} = [E^+(M) - E^+(M^+)] + [E(M^+) - E(M)]$$
$$\lambda_{electron} = [E^-(M) - E^-(M^-)] + [E(M^-) - E(M)]$$

Table 4 Molecular orbital energy levels (eV) for all the investigated porphyrin derivatives

	ZnQMA	A	B	C	D	E
LUMO+1	−2.36	−2.49	−2.29	−2.21	−2.40	−2.33
LUMO	−2.71	−2.71	−2.72	−2.41	−2.74	−2.67
HOMO	−5.30	−5.09	−4.95	−5.07	−5.08	−4.84
HOMO−1	−5.31	−5.29	−5.16	−5.20	−5.26	−5.17
Gap	2.58	2.38	2.23	2.66	2.34	2.17

Table 5 Computed absorption wavelengths (nm), oscillator strengths (*f*), two highest electronic transition configurations for the main optical transitions in B and Q bands, and fluorescence maxima (nm) in solvent CH_2Cl_2 with respect to the available experimental data (in parentheses) for every considered compound

Molecules	λ_{abs} (nm)	*f*	Composition	λ_{flu} (nm)
ZnQMA	586.7 $(578)_{exp}$	0.0313	H−1 → L (0.62), H → L+1 (0.28), H → L (−0.18)	673.1 $(645)_{exp}$
	405.6 $(415)_{exp}$	1.8839	H−1 → L+1 (0.43), H−1 → L+1 (0.43), H → L+2 (−0.41)	
A	683.6	0.0276	H → L (0.67), H → L+2 (−0.14), H−1 → L+1 (−0.13)	728.4
	416.3	1.3854	H−3 → L (0.53), H−1 → L+2 (0.33), H → L+1 (−0.20)	
B	730.7	0.0866	H → L (0.68), H−2 → L (−0.14)	722.0
	433.2	1.4829	H−1 → L+1 (0.44), H → L+2 (−0.43), H−2 → L+2 (0.24)	
C	566.7	0.0416	H → L (0.59), H−1 → L+1 (0.38)	578.5
	433.9	1.2043	H → L+1 (0.38), H−1 → L (0.35), H−1 → L+1 (−0.31)	
D	667.5	0.1408	H → L (0.66), H−2 → L (−0.17), H−1 → L+1 (−0.14)	805.5
	425.4	1.2916	H → L+2 (0.48), H−1 → L+1 (0.37), H−2 → L+2 (−0.24)	
E	727.5	0.1053	H → L (0.69)	
	417.7	0.7437	H−3 → L (0.41), H−2 → L+1 (−0.34), H−1 → L +2 (−0.30)	

Only selected transitions with enough oscillator strength around the main peak are included (H stands for HOMO and L for LUMO)

E^+, E, and E^- represent the energies of the cation, neutral, and anion species based on their lowest energy geometries, respectively, while (M^+), (M) and (M^-) denote their optimized structures at corresponding ion states. For example, $E^{+/-}$(M) is the energy of a cation/anion calculated with the optimized structure of the neural molecule M.

Our calculations give $\lambda_{electron} = 0.19$, 0.22, 0.17, 0.10, 0.09 and 0.14 eV for **ZnQMA**, **A**-**E**, respectively, and the value of λ_{hole} is in the same order of magnitude (0.15, 0.17, 0.22, 0.17, 0.09 and 0.28 eV for **ZnQMA**, **A**-**E**, respectively). The lower the λ value, the bigger the charge-transport rate. Our results show that the $\lambda_{electron}$s for **B**-**E** are smaller than that for **ZnQMA**, but λ_{hole} only for **D** is smaller than that for **ZnQMA**. The difference between λ_{hole} and $\lambda_{electron}$ for **D** is the smallest in all the investigated compounds. Therefore, our computations suggest that molecule **D** not only has higher electron and hole-transfer rate than **ZnQMA** but also has improved charge-transfer balance performance, which is crucial in achieving a high quantum efficiency in optoelectronic devices.

3.2.3 *Absorption and fluorescence spectra of the isolated molecules*

To understand electronic transitions of all the studied porphyrin derivatives, TDDFT calculations on the absorption and emission spectra in solvent (CH_2Cl_2) have been performed. The calculated wavelengths from absorption spectra, oscillator strength, main configurations, and fluorescence maximum wavelength are listed in Table 5. Simulated electronic absorption spectra plots of molecules are shown in Fig. 3.

As shown in Table 5, a reasonable agreement between the experimental and calculated bands of **ZnQMA** can be noticed. We stress that we interested here in relative band shifts upon modifying the fixed aromatic rings, rather than in absolutely reproducing excitation energies. The same trend of the Q-band positions of these complexes is observed as that of the HOMO–LUMO gaps from Kohn–Sham orbital energies shown in Table 4. The absorption spectra in both Soret and Q bands for **A**, **B**, **D**, and **E** exhibit red shifts to some extent with respect to that of **ZnQMA**. By looking at Table 5 and Fig. 2, one can find

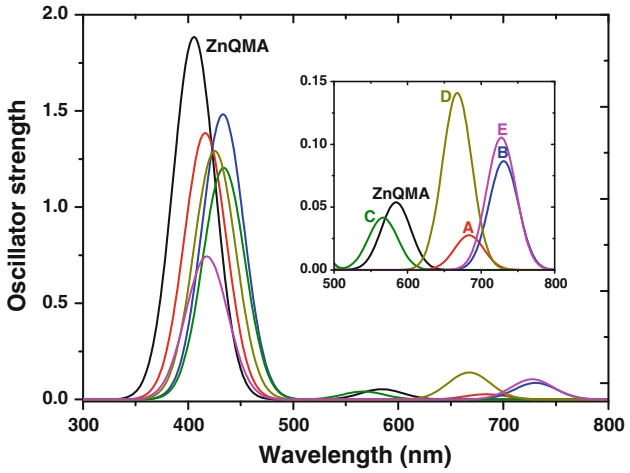

Fig. 3 Simulated absorption spectra of **ZnQMA** (*black*), *A* (*red*), *B* (*blue*), *C* (*green*), *D* (*olive*), *E* (*magenta*) calculated in CH_2Cl_2 solution

that the Q bands of all the molecules correspond to a $\pi \rightarrow \pi^*$ transition with a strong HOMO-to-LUMO character. The HOMO is mainly contributed from atomic orbitals of porphyrin ring and fixed aromatic rings, while in the LUMO, the density of electron clouds around carboxylic acids apparently increases. So the absorption of Q bands mainly comes from the intramolecular charge transfer.

As depicted in Table 5 and Fig. 3, the strength of Q band for molecules **B**, **D**, and **E** is significantly increased in comparison with that for **ZnQMA**. Previous investigations indicate that the main reason of the limited performance of porphyrin-sensitized TiO_2 cells is that porphyrins possess relatively weak Q bands compared with intense Soret bands. From our calculations, the designed compounds **B**, **D**, and **E** are supposed to display better light-harvesting properties in Q bands than **ZnQMA**.

Concerning fluorescence, the computed emission maximum for **ZnQMA** is in good agreement with the experimental data. The computed Stokes shifts (the difference between the absorption maximum and emission maximum) indicate that the largest shift is obtained for molecule **D**, which is larger than that of **ZnQMA** by ca. 50 nm. Combining Table 3 with Table 5, one can find the large structural relaxation at the excited state is responsible for the highest Stokes shift for **ZnQMA**.

3.3 Effects of semiconductor

In the dye-sensitized systems, anchoring groups such as carboxylic acid groups are known to be spontaneously adsorbed onto TiO_2 surfaces. They form bidentate chelating, bidentate bridging, and/or monodentate ester-type binding with TiO_2 surfaces depending on the experimental conditions [70]. In the present work, we have just optimized **ZnQMA** and molecule **D** bound up with TiO_2 cluster in the two kinds of forms, bidentate chelating and monodentate ester-type, due to the relatively small size of our TiO_2 cluster. The relaxed compounds with the full optimization are shown in Fig. 4. Both **ZnQMA** and molecule **D** are adsorbed dissociatedly on the surfaces of TiO_2 clusters. As shown in Fig. 4, the optimized Ti–O bond lengths (1.881, 1.997, and 2.064 Å) in **D**–TiO_2 complexes are shorter than those (1.890, 2.013, and 2.084 Å) in **ZnQMA**–TiO_2 complexes, respectively. The slightly shorter Ti–O bond lengths calculated for **D**–TiO_2 complexes point toward a stronger interaction of the dye with the titania surface compared to **ZnQMA**–TiO_2 complexes. We computed the bidentate adsorption mode to be energetically favored compared to the monodentate one by 0.22 and 0.29 eV in **ZnQMA**–TiO_2 and **D**–TiO_2 systems, respectively, which well confirms the experimental results observed by X-ray photoelectron spectroscopy [40, 41]. So we will concentrate on the electronic properties of the dye–TiO_2 systems with bidentate adsorption mode in the following discussion.

The computed $(TiO_2)_8$ cluster has a HOMO–LUMO gap of 4.08 eV, which is close to the calculated gap of 3.78 eV in $(TiO_2)_{38}$ nanocluster [52]. Inspecting the calculated

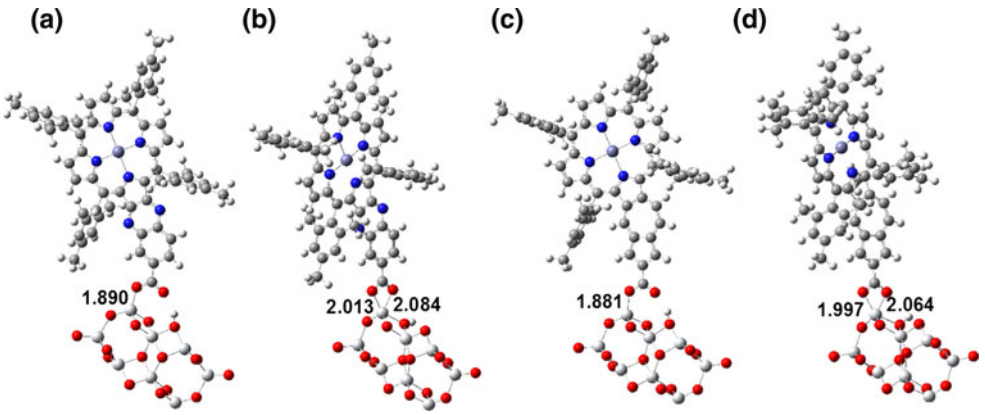

Fig. 4 Optimized geometries of dye–(TiO_2) (cluster) complexes. Zn, Ti, O, N, C, and H atoms are in purple, *light gray*, *red*, *blue*, *dark gray*, and *white*, respectively; **a ZnQMA**–TiO_2–monodentate-type, **b ZnQMA**–TiO_2–bidentate-type, **c D**–TiO_2–monodentate-type, **d D**–TiO_2–bidentate-type

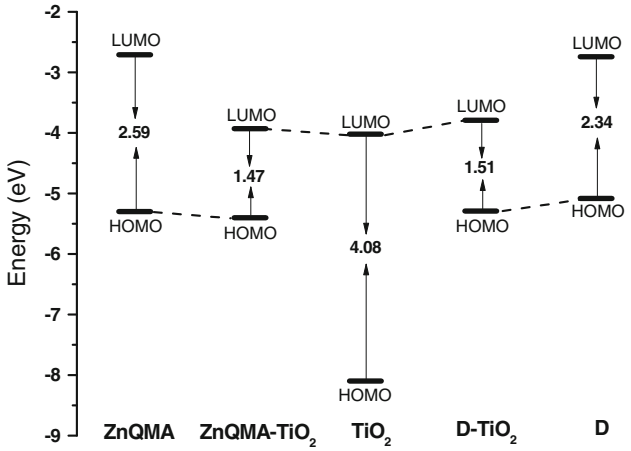

Fig. 5 Schematic energy diagram of the non-interacting and interacting dyes **ZnQMA** and **D** and of the $(TiO_2)_8$ cluster

electronic structure for the interacting dye–semiconductor systems shown in Fig. 5, one can notice that the HOMO–LUMO gaps of **ZnQMA**–TiO_2 and **D**–TiO_2 systems are 1.47 and 1.51 eV, respectively, which are drastically reduced with respect to those of the non-interacting systems. The HOMOs in the interacting systems have almost exactly the same alignment of the energy levels as those in the isolated dye molecules, and the LUMOs of them are energetically close to the LUMO of TiO_2 clusters.

To simulate the absorption spectra for the two interacting systems, we performed TDDFT calculations on these complexes including solvation effects. The computed absorption spectra are red-shifted as compared to the isolated dye molecule in solution for both **ZnQMA**–TiO_2 (630.3 vs. 586.7 nm) and **D**–TiO_2 systems (705.3 vs. 667.5 nm), reflecting the stronger interaction of the dye with the semiconductor. In Fig. 6, some relevant molecular orbitals for the lowest energy absorption of **ZnQMA**–TiO_2 and **D**–TiO_2 systems are shown. These orbitals have been chosen because they are the most important in contributing to the lowest-energy band. For **ZnQMA**–TiO_2, the band is made of several optical transitions, including HOMO−1 → LUMO, HOMO → LUMO, and HOMO → LUMO+4. As shown in Fig. 6, the occupied orbitals are all mainly localized on **ZnQMA**. The unoccupied orbitals are well localized on the $(TiO_2)_8$ cluster. For **D**–TiO_2, the similar transition pattern has been obtained. The occupied orbitals that contribute most to the lowest-energy band are HOMO, HOMO−1, and HOMO−2, which are localized on **D**. The most important unoccupied orbitals LUMO and LUMO+4 are localized on the $(TiO_2)_8$ cluster. So, for the two interacting porphyrin-TiO_2 systems, our calculations predict that a direct photoexcitation from the dye HOMOs to the semiconductor LUMOs occurs [71–73].

4 Conclusions

In this paper, we have utilized DFT–TDDFT approach to investigate β, β'-edge-fused zinc porphyrins with different aromatic moieties. The ground states, the lowest singlet states, excitations, and electronic structures of all the isolated molecules have been studied at the of B3LYP/6-31G(d) level. The agreements between experimental and theoretical geometry parameters, absorption, and emission spectra are reasonably good. We have found that β, β'-edge-fused zinc porphyrin with azulene ring (**D**) exhibits smaller HOMO–LUMO energy gap, higher electron- and hole-transfer rates, and much stronger absorption in Q band than those of **ZnQMA**, which possesses the high photoelectric conversion efficiency 6.3%. The computed results propose that direct photoexcitation from the dye HOMOs to the semiconductor LUMOs occurs in the studied porphyrin–TiO_2 systems. Our calculation indicates that the studied molecule **D** has stronger interaction with TiO_2 cluster than the reported **ZnQMA**. Therefore, our results show that the designed molecule **D** is a promising

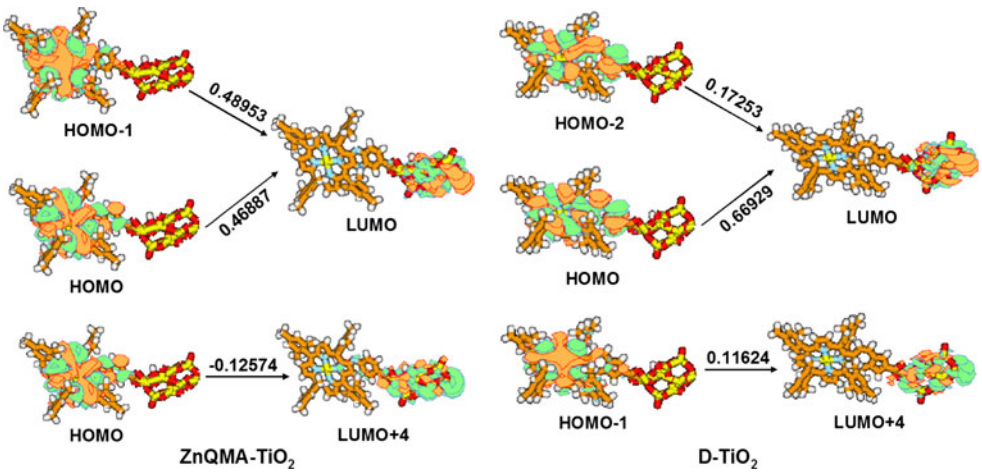

Fig. 6 Single-electron transitions with |CI coefficient| > 0.1 in the TDDFT calculations for the lowest energy absorption of **ZnQMA**–TiO_2 and **D**–TiO_2 systems

candidate to challenge the current record of **ZnQMA** in the DSSC. Further experimental research to check the prediction of β, β'-edge-fused zinc porphyrin with azulene ring–sensitized solar cells is demanding.

Acknowledgments Dr. Dong gratefully acknowledges the financial support from Liaoning Normal University. Dr. Zhou appreciates the funding support by Technology Foundation for selected Overseas Chinese Scholar from Ministry of Personnel of China and the "100-Talents-Program" of the Dalian Institute of Chemical Physics, Chinese Academy of Sciences. Professor Jiang is grateful to the National Science Foundation of China under Grant 20873056 for financial support.

References

1. O'Regan B, Grätzel M (1991) Nature 353:737–740
2. Hagfeldt A, Grätzel M (1995) Chem Rev 95:49–68
3. Grätzel M (2001) Nature 414:338–344
4. Kamat PV (2007) J Phys Chem C 111:2834–2860
5. Nazeeruddin MK, Pechy P, Renouard T, Zakeeruddin SM, Humphry- Baker R, Comte P, Liska P, Cevey L, Costa E, Shklover V, Spiccia L, Deacon GB, Bignozzi CA, Grätzel M (2001) J Am Chem Soc 123:1613–1624
6. Nazeeruddin MK, De Angelis F, Fantacci S, Selloni A, Viscardi G, Liska P, Ito S, Takeru B, Grätzel M (2005) J Am Chem Soc 127:16835–16847
7. Gao F, Wang Y, Zhang J, Shi D, Wang M, Humphry-Baker R, Wang P, Zakeeruddin SM, Grätzel M (2008) Chem Commun 44:2635–2637
8. Chen C-Y, Wang M, Li J-Y, Pootrakulchote N, Alibabaei L, Ngoc-le C, Decoppet J-D, Tsai J-H, Grätzel C, Wu C-G, Zakeeruddin SM, Grätzel M (2009) ACS Nano 3:3103–3109
9. Ooyama Y, Harima Y (2009) Eur J Org Chem 2009:2903–2934
10. Mishra A, Fischer MKR, Bäuerle P (2009) Angew Chem Int Ed 48:2474–2499
11. Hara K, Sayama K, Ohga Y, Shinpo A, Suga S, Arakawa H (2001) Chem Commun 37:569–570
12. Furube A, Katoh R, Hara K, Sato T, Murata S, Arakawa H, Tachiya M (2005) J Phys Chem B 109:16406–16414
13. Wang Z-S, Cui Y, Hara K, Dan-oh Y, Kasada C, Shinpo A (2007) Adv Mater 19:1138–1141
14. Wang Z-S, Cui Y, Dan-oh Y, Kasada C, Shinpo A, Hara K (2008) J Phys Chem C 112:17011–17017
15. Hara K, Kurashige M, Ito S, Shinpo A, Suga S, Sayama K, Arakawa H (2003) Chem Commun 39:252–253
16. Kitamura T, Ikeda M, Shigaki K, Inoue T, Anderson NA, Ai X, Lian T, Yanagida S (2004) Chem Mater 16:1806–1812
17. Im H, Kim S, Park C, Jang S-H, Kim C-J, Kim K, Park N-G, Kim C (2010) Chem Commun 46:1335–1337
18. Wang Z-S, Li F-Y, Huang C-H, Wang L, Wei M, Jin L-P, Li N-Q (2000) J Phys Chem B 104:9676–9682
19. Chen Y-S, Li C, Zeng Z-H, Wang W-B, Wang X-S, Zhang B-W (2005) J Mater Chem 15:1654–1661
20. Tan S, Zhai J, Fang H, Jiu T, Ge J, Li Y, Jiang L, Zhu D (2005) Chem Eur J 11:6272–6276
21. Choi H, Baik C, Kang SO, Ko J, Kang M-S, Nazeeruddin MK, Grätzel M (2008) Angew Chem Int Ed 47:327–330
22. Zhang G, Bala H, Cheng Y, Shi D, Lv X, Yu Q, Wang P (2009) Chem Commun 45:2198–2200
23. Horiuchi T, Miura H, Uchida S (2003) Chem Commun 39:3036
24. Kuang D, Uchida S, Humphry-Baker R, Zakeeruddin SK, Grätzel M (2008) Angew Chem Int Ed 47:1923–1927
25. Shibano Y, Umeyama T, Matano Y, Imahori H (2007) Org Lett 9:1971–1974
26. Li C, Yum J-H, Moon S-J, Herrmann A, Eickemeyer F, Pschirer NG, Erk P, Schöneboom J, Müllen K, Grätzel M, Nazeeruddin MK (2008) ChemSusChem 1:615–618
27. Chen Y, Zeng Z, Li C, Wang W, Wang X, Zhang B (2005) New J Chem 29:773–776
28. Yum J-H, Walter P, Huber S, Rentsch S, Geiger T, Nüesch F, De Angelis F, Grätzel M, Nazeeruddin MK (2007) J Am Chem Soc 129:10320–10321
29. Burke A, Ito S, Snaith H, Bach U, Kwiatkowski J, Grätzel M (2008) Nano Lett 8:977–981
30. Reddy PY, Giribabu L, Lyness C, Snaith HJ, Vijaykumar C, Chandrasekharam M, Lakshmikantam M, Yum J-H, Kalyanasundaram K, Grätzel M, Nazeeruddin MK (2007) Angew Chem Int Ed 46:373–376
31. O'Regan BC, López-Duarte I, Martinez-Diaz MV, Forneli A, Albero J, Morandeira A, Palomares E, Torres T, Durrant JR (2008) J Am Chem Soc 130:2906–2907
32. Cid J-J, García-Iglesias M, Yum J-M, Eorneli A, Albero J, Martinez- Ferrero E, Vázquez P, Grätzel M, Nazeeruddin MK, Palomares E, Torres T (2009) Chem Eur J 15:5130–5137
33. Tanaka M, Hayashi S, Eu S, Umeyama T, Matano Y, Imahori H (2007) Chem Commun 2069–2071
34. Campbell WM, Jolley KW, Wagner P, Wagner K, Walsh PJ, Gordon KC, Schmidt-Mende L, Nazeeruddin MK, Wang Q, Grätzel M, Officer DL (2007) J Phys Chem C 111:11760–11762
35. Balanay MP, Dipaling CVP, Lee SH, Kim DH, Lee KH (2007) Sol Energy Mater Sol Cells 91:1775–1781
36. Balanay MP, Kim DH (2008) Phys Chem Chem Phys 10:5121–5127
37. Ma R, Guo P, Cui H, Zhang X, Nazeeruddin MK, Grätzel M (2009) J Phys Chem A 113:10119–10124
38. Ma R, Guo P, Yang L, Guo L, Zhang X, Nazeeruddin MK, Grätzel M (2010) J Phys Chem A 114:1973–1979
39. Bessho T, Zakeeruddin SM, Yeh C-Y, Diau EW-G, Grätzel M (2010) Angew Chem Int Ed 49:6646–6649
40. Eu S, Hayashi S, Umeyama T, Matano Y, Araki Y, Imahori H (2008) J Phys Chem C 112:4396–4405
41. Kira A, Matsubara Y, Iijima H, Umeyama T, Matano Y, Ito S, Niemi M, Tkachenko NV, Lemmetyinen H, Imahori H (2010) J Phys Chem C 114:11293–11304
42. Muranaka A, Yonehara M, Uchiyama M (2010) J Am Chem Soc 132:7844–7845
43. Becke AD (1993) J Chem Phys 98:5648–5652
44. Lee C, Yang W, Parr RG (1988) Phys Rev B 37:785–789
45. Lynch BJ, Fast PL, Harris M, Truhlar DG (2000) J Phys Chem A 104:4811–4815
46. Adamo C, Barone V (1999) J Chem Phys 110:6158–6170
47. Frish MJ et al (2009) *Gaussian 09*, revision A.02. Gaussian Inc., Wallingford
48. Hariharan PC, Pople JA (1973) Theor Chim Acta 28:213–222
49. Angeli C, Pastore M, Cimiraglia C (2007) Theor Chem Acc 117:743–754
50. Stratmann RE, Scuseria GE, Frisch MJ (1998) J Chem Phys 109:8218–8224
51. Tomasi J, Mennucci B, Cammi R (2005) Chem Rev 105:2999–3094
52. De Angelis F, Tilocca A, Selloni A (2004) J Am Chem Soc 126:15024–15025
53. De Angelis F, Fantacci S, Selloni A, Nazeeruddin MK, Gräzel M (2010) J Phys Chem C 114:6054–6061
54. De Angelis F, Fantacci S, Mosconi E, Nazeeruddin MK, Gräzel M (2011) J Phys Chem C 115:8825–8831
55. Guo Z, Liang W, Zhao Y, Chen G (2008) J Phys Chem C 112:16655–16662

56. Sánchez-de-Armas R, López JO, San-Miguel MA, Sanz JF (2010) J Chem Theory Comput 6:2856–2865
57. Peng B, Yang S, Li L, Cheng F, Chen J (2010) J Chem Phys 132:034305
58. Pastore M, Mosconi E, De Angelis F, Grätzel M (2010) J Phys Chem C 114:7205–7212
59. Nemykin VN, Basu P (2001) Virtual molecular orbital description program (VMOdes), Department of Chemistry, Duquesne University, Pittsburgh, PA
60. Scheidt WR, Kastner ME, Hatano K (1978) Inorg Chem 17:706–710
61. Golder AJ, Povey DC (1990) Acta Crystallogr Sect C Cryst Struct Commun 46:1210–1212
62. Guillemoles J-F, Barone V, Joubert L, Adamo C (2002) J Phys Chem A 106:11354–11360
63. Fantacci S, De Angelis F, Wang J, Bernhard S, Selloni A (2004) J Am Chem Soc 126:9715–9723
64. Gouterman M (1961) J Mol Spectrosc 6:138–163
65. Hagberg DP, Edvinsson T, Marinado T, Boschloo G, Hagfeldt A, Sun L (2006) Chem Comm 42:2245–2247
66. Epstein AJ, Lee WP, Prigodin VN (2001) Synth Met 117:9–13
67. Hutchison GR, Ratner MA, Marks TJ (2005) J Am Chem Soc 127:2339–2350
68. Marcus RA (1956) J Chem Phys 24:966–978
69. Marcus RA (1993) Rev Mod Phys 65:599–610
70. Vittadini A, Selloni A, Grätzel M (2000) J Phys Chem B 104:1300–1306
71. Duncan WR, Craig CF, Prezhdo OV (2007) J Am Chem Soc 129:8528–8534
72. Szarko JM, Neubauer A, Bartelt A, Socaciu-Siebert L, Birkner F, Schwarzburg K, Hannappel T, Eichberger R (2008) J Phys Chem C 112:10542–10552
73. De Angelis F (2010) Chem Phys Lett 493:323–327